NEW APPROACHES TO PROBLEMS OF FLUID FLOW IN FRACTURED ROCK MASSES

Paul A. Witherspoon, Yvonne W. Tsang,
Jane C. S. Long, and Jahandar Noorishad

Lawrence Berkeley laboratory,
University of California
Berkeley, California 94720

Proceedings of the 22nd U.S. Symposium on Rock Mechanics: Rock Mechanics from Research to Application held at Mass. Inst. of Tech., June 28-July 2, 1981 compiled by H.H. Einstein

INTRODUCTION

Investigations on the factors that control the movement of fluids in the underground inevitably become involved with fractured rock masses. In the petroleum industry, it was recognized long ago that the presence of fractures, either natural or man made, is crucial to the economics of the recovery methods to be employed in many oil fields. The development of groundwater resources is likewise often dependent on the presence of fractures to provide a drainage system in low permeability rocks. Geotechnical engineers have been faced with difficult problems when designing and constructing large engineering works in fractured rocks; catastrophic failures of large dams provide evidence of the magnitude of their problems. The leakage problems that have resulted when natural fractures were not detected in developing projects for underground storage of petroleum hydrocarbons are still another kind of evidence of the importance of fracture systems. The current problem of evaluating migration of aqueous solutions of radionuclides through crystalline rock masses where the movement will be controlled by the discontinuities is a critical issue in the design of nuclear waste repositories. These examples simply serve to illustrate the fact that the fractures play a key role in understanding the flow behavior of rock systems.

Despite the importance of this problem and the great amount of investigation by many workers, much remains to be done in developing a complete understanding of the factors that control fluid movement through fractured rocks. The range of subject matter covered by the papers presented in Topic Area 1 of this symposium gives a good indication of the complex problems that face earth scientists.

We shall address three different aspects of this problem in an effort to describe some investigations currently underway in this laboratory. The first part of this paper is an attempt to develop an expression for fluid flow in a deformable fracture. Our approach to this problem of the hydromechanical behavior of a deformable fracture differs from that of Gangi (1978) although we both have a common starting point, the roughness of the fracture surface. The second part has to do with the problem of how to treat flow through networks of fractures. It is customary to consider a discontinuous rock mass by some equivalent porous medium but this raises some important questions that will be discussed. The third part will present the most recent results by our group to develop a fully coupled finite element code for flow through fractured porous media subject to thermal, hydraulic and mechanical stresses.

HYDROMECHANICS OF FLOW IN A SINGLE FRACTURE

We have developed a simple physical model to understand the effect of normal stress on flow through a single rough walled fracture. In order to gain a fundamental understanding of the problem, we have focussed on the physical mechanisms and have excluded the use of arbitrary fitting parameters. A single fracture is considered to be composed of a collection of voids, and the closure of the fracture under stress to result from the deformation of these voids. From such a model, the macroscopic measurable quantities, such as the normal stress and corresponding normal fracture displacements, can be correlated to the geometrical characterization of a rough walled fracture. The effect of roughness is incorporated into the usual parallel plate model of a fracture, and the flow rate as a function of normal stress is predicted and validated against laboratory data on granite and basalt.

Solutions of the Navier Stokes equation show (Boussinesq, 1868; Bear, 1972) that steady, laminar flow through two smooth parallel plates separated by a constant distance b obeys the cubic law, that is, the flow rate is proportional to b^3. The cubic law has been shown to hold down to apertures of 0.2 μm in open fractures made of optically smooth glass (Romm, 1966). We have shown (Tsang and Witherspoon, 1981) that an equivalent cubic law may be used for a rough walled fracture if the constant value for the aperture is replaced by a statistical average. This implies that the hydrological property of a rough walled fracture may be suitably modeled by a mathematical aperture distribution function.

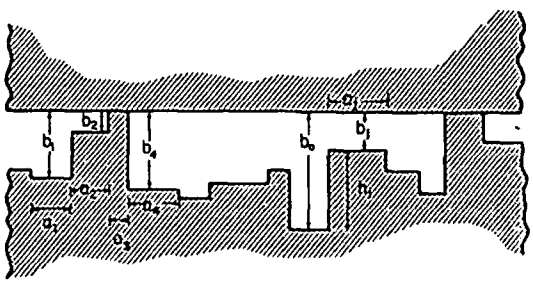

Fig. 1 Schematic representation of a fracture by an asperity model.

Fig. 1 shows such a schematic representation for a fracture, which consists of a smooth top slab and a rough bottom slab with asperities of different heights (h_j). The configuration of asperities gives rise to a fracture with variable aperture b_j. The problem is then to develop an asperity function that is a correct mathematical expression for the variability of the real, physical fracture.

Theoretical Development

Geometrically, a single rough walled fracture may be envisioned either as a collection of voids or as an array of asperities (Fig. 2). Under increasing

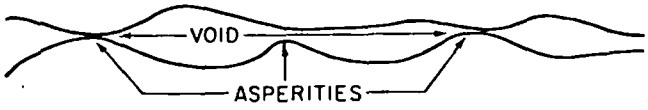

Fig. 2 Schematic representation of a fracture by either the asperity or the void model.

normal stress, more asperities come in contact and the average distance between points of contact decreases. Though an asperity description for a fracture seems to be a natural candidate for the study of flow through fractures, we find that the void description is better suited to the interpretation of the mechanical property of a single fracture under stress. By considering the closure of a single fracture as resulting from the shortening of the average crack length of the voids, we were able to arrive at an asperity function consistent with mechanical measurements of fracture displacement and applied normal stress.

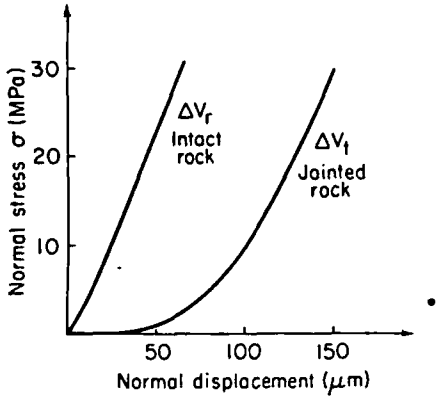

Fig. 3 Typical normal stress-displacement behavior for intact and jointed rock.

Given measurements of normal stress displacement for both intact and jointed rock such as those shown in Fig. 3, we may define both the intrinsic Young's modulus, E, for the intact rock and the effective Young's modulus, E_{eff}, for the jointed rock from the respective slopes of the stress-displacement curves:

$$E(\sigma,\Delta V_r) = \frac{1}{\ell}\frac{d\sigma}{d\Delta V_r} \qquad (1)$$

$$E_{eff}(\sigma,\Delta V_t) = \frac{1}{\ell}\frac{d\sigma}{d\Delta V_t} \qquad (2)$$

At low stresses, the effective Young's modulus E_{eff} of the jointed rock is much smaller than that of the solid rock. As stress is increased, E_{eff} approaches the value of E for the solid rock.

Consider first the geometry of one elliptic flat crack of length 2d enclosed in a rock volume of $u = \Delta x\Delta y\Delta z$. Following closely the formulation of Walsh (1965), one can show that for a rock with a collection of voids, all with the same orientation as the one shown in Fig. 4, the effective modulus E_{eff}

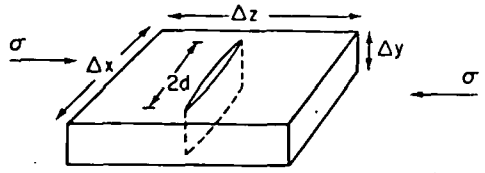

Fig. 4 Geometry of a flat elliptic crack in in rock block under stress.

of the rock with voids is related to the intrinsic rock modulus E by:

$$\frac{1}{E_{eff}} = \frac{1}{E} + \frac{4\pi\langle d^3\rangle}{E\langle u\rangle}, \qquad (3)$$

where both the half-crack length cubed and the volume enclosing each void have been averaged over all the voids in the sample. This expression is not sensitive to the actual shape of the void. The second term on the right-hand side of (3) arises from the strain energy associated with the cracks. Since (3) applies to a physical situation of sparse voids, the effect of the voids on the elastic modulus is expected to be small. Then the property of the rock medium in which the voids are situated may be described by Young's modulus for the intact rock, and therefore the same modulus E appears in the strain energy term associated with the cracks.

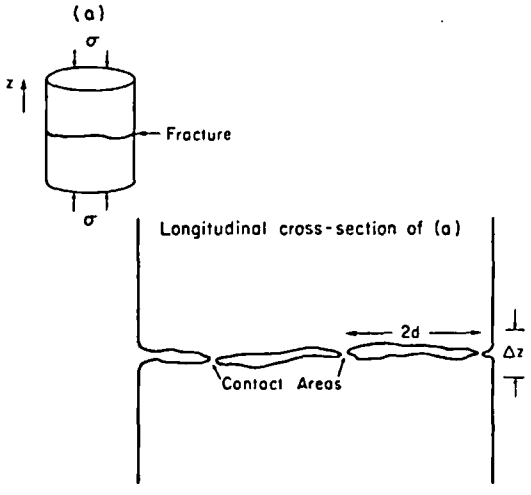

Fig. 5 Representation of single horizontal fracture by an array of voids.

If we were to consider one single horizontal fracture as a collection of voids, the physical situation will be as shown in Fig. 5. Here the voids are dense and the void ratio is large. Only a small fraction of the total fracture area is in contact. To describe the effective modulus E_{eff} of the fractured rock in the vicinity of the fracture, (3) may be modified to:

$$\frac{1}{E_{eff}} = \frac{1}{E} + \frac{4\pi\langle d^3\rangle}{E_{eff}\langle u\rangle}, \qquad (4)$$

where (4) now includes E_{eff} in the last term. When the voids are large in number and close in proximity, the void-void interaction is no longer negligible as is assumed in the derivation of (3). Since it is difficult if not impossible to account for this interaction in the calculation of strain energies, we make a plausibility argument to lump the effect of the interaction by introducing E_{eff} in the last term of (4). The argument being that due to the high void ratio, the property of the rock medium is better represented by the effective modulus of the fractured rock than by the modulus of the intact rock.

Suppose there are M_v voids in the fracture with a total cross sectional area A. then the average volume enclosing each crack may be written as:

$$\langle u \rangle = \frac{A\,\Delta z}{M_v} \tag{5}$$

where Δz is a thickness around the fracture within which E_{eff} is applicable (see Fig. 5). Since the rock fracture is represented by a collection of voids, one expects the contact area of the fracture walls to be small such that the total void area is almost identical to the total fracture cross section area A. Therefore:

$$\langle (2d)^2 \rangle\, M_v \approx A \ . \tag{6}$$

In addition, for a spatially random collection of M_v voids, $\langle d^3 \rangle \approx \langle d^2 \rangle \langle d \rangle$ and (4) may now be written approximately as:

$$\frac{E_{eff}}{E} \approx 1 - \frac{\pi \langle d \rangle}{\Delta z} \tag{7}$$

Equation 7 gives a useful relationship between the two moduli and the average half-crack length $\langle d \rangle$ which characterizes the rough fracture at different levels of stress.

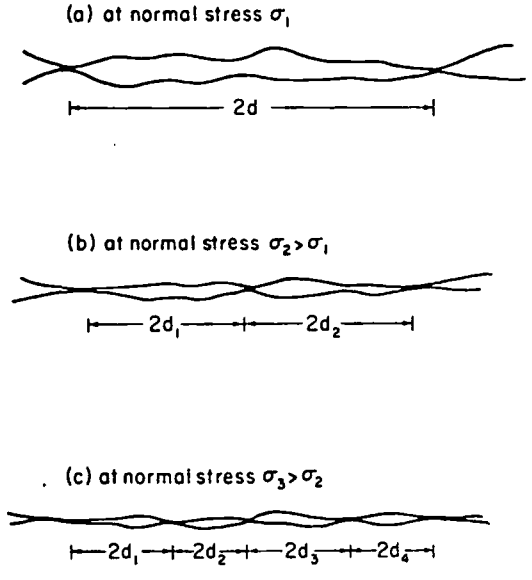

Fig. 6 Deformation of voids in a sequence of increasing normal stresses.

The physical picture implied by (7) is illustrated schematically in Fig. 6, which is an attempt to portray a portion of fracture shown in Fig. 5 at different stages of normal stress. The crack length 2d is defined as the distance between two adjacent areas where the two fracture surfaces come into contact. These areas of contact are simply the asperities as shown in Fig. 2. Under increasing load, the deformation of the voids causes more asperities to come in contact, and leads to a decrease in the average crack length. This process results in a gradual increase of the effective modulus with increasing normal stress according to (7). The average crack length $2\langle d \rangle$ continues to decrease as the voids deform until the term $\langle d \rangle / \Delta z$ becomes negligibly small compared to 1, at which point the jointed rock will exhibit an effective modulus identical to that of the intrinsic modulus.

We therefore attribute the "softness" of a jointed rock to an average crack length that initially is relatively long and the stiffening of the jointed rock under compression to the shortening of this average crack length. This differs from Gangi's (1978) "bed of nails" model, in which he ascribes the closure of a fracture to the elastic compression of the "nails" or "asperities". In Gangi's model, the "softness" of the fracture is said to result from the small number of asperities that are in contact. These areas therefore sustain much higher stresses than that measured by the total load divided by the total fracture area. As a result, the strain of these asperities in contact is expected to be larger than the strain in an intact rock under the same load.

However, when we apply such an asperity model to both the flow data and stress-strain measurements in a granite fracture [Iwai, 1976], we found that in order to obtain a result that is quantitatively compatible with the data, we had to assume that the total area of all the asperities that are in contact with the top slab (Fig. 1) took on a value of less than .001 of the total fracture area at an applied stress level of 20 Mpa. The experimental measurement [Iwai, 1976] gives a value between .1 to .2 for the contact area of the fracture at the same stress level. The discrepancy of two orders of magnitude between a parameter in the theory and measurement implies that the physical fracture system appears to be much "softer" than that described by the asperity model. On the other hand, the alternate mechanism proposed above, where the closure of the fracture under normal stress is ascribed to the deformation of voids, does predict a very soft elastic property at low stress. It also predicts a gradual increase of Young's modulus with stress, and a correct contact area in accordance with the laboratory measurment.

It is clear from Fig. 6 that one may view the sequence (a) (b) (c) either as a decrease in the average crack length $2\langle d \rangle$ or as an increase in the number N_c of areas in contact under increasing load. For a rough-walled fracture, we shall describe the former process as a "void model" and the latter process as an "asperity model." For a spatially random distribution of voids or asperities, N_c varies inversely with $\langle d \rangle$. Given elastic stress measurements, it is evident from (7) that the relative average crack length $2\langle d \rangle$ as a function of stress or fracture displacement can be calculated, and therefore, N_c may be deduced.

The number of contact areas, N_c, is the key to aperture distribution. Fig. 1 represents a rough-

walled fracture as an array of asperities of varying heights h_j. At zero applied stress, the maximum possible aperture is b_o, which corresponds to an asperity of zero height. With applied axial stress, the fracture closure ΔV results in a downward displacement of the top slab. At nonzero stresses, the aperture which corresponds to each asperity of height h is:

$$b = \begin{cases} (b_o - \Delta V - h) & h < (b_o - \Delta V) \\ o & h \geq (b_o - \Delta V) \end{cases} \quad (8)$$

Let n(h) denote the asperity height frequency distribution function which characterizes the fracture prior to loading. Then N_c, the total number of asperities in contact at any stress, is:

$$N_c(\Delta V) = \int_{b_o - \Delta V}^{b_o} n(h)\, dh. \quad (9)$$

It is clear from (9) that the asperity height distribution function, n(h), can be obtained from the derivative of N_c. For a given set of stress displacement measurements, it is possible only to deduce the change in $\langle d \rangle / \Delta z$ relative to its value at zero applied stress from (7). This implies that N_c and in turn n(h) can only be determined to within some constant multiplier, because the value of b_o is not known. If the contact area as a fraction of the total fracture area is known to be ω at a specified deformation ΔV, then:

$$\omega = \frac{N_c(\Delta V)}{N_c(b_o)} \quad (10)$$

and b_o is readily determined if a functional form exists for $N_c(\Delta V)$.

We have shown (Tsang and Witherspoon, 1981) that if the aperture variation of the fracture is spatially random, the equivalent cubic law for flow through a rough walled fracture may be written as:

$$\frac{Q}{\Delta \phi} = C \langle b^3 \rangle \quad (11)$$

where C is a proportionality constant that depends on the macroscopic fracture dimensions and properties of the fluid. The statistical average for the variation in aperture may therefore be computed from:

$$\langle b^3(\Delta V, \sigma) \rangle = \frac{\int_0^{b_o - \Delta V} (b_o - \Delta V - h)^3 n(h)\, dh}{\int_0^{b_o} n(h)\, dh} \quad (12)$$

Once the normal stress displacement measurements and an estimated contact area of the fracture at any stress are known, flow through the rough fracture may be calculated from (12).

Application to Laboratory Data

We used results from Iwai's (1976) laboratory investigations on the mechanical and hydrological properties of tension fractures in samples of basalt and granite to test the validity of our physical theory. Iwai measured normal displacements for both intact and jointed rock at normal stresses up to 20MPa, and he also estimated the contact area within the fracture to be 10 to 20% of the total fracture area at maximum stress. Figure 7 shows how his results for radial flow of water through a single fracture in basalt decreased with increasing normal stress during the first loading cycle. Based on his fracture displacements, we used (12) to determine average apertures and then computed flow rates from (11) for fractional contact areas of 10, 15, and 20%. The smooth curves on Figure 7 show how the theoretical results compare with Iwai's experimental data.

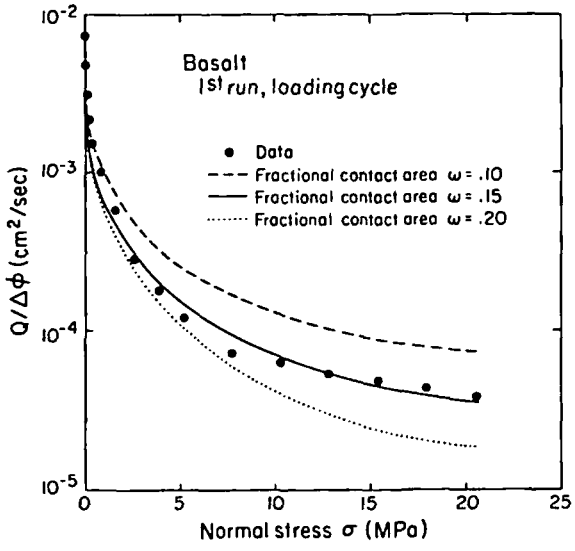

Fig. 7 Experimental and theoretical flow as a function of normal stress in basalt.

In analyzing Iwai's (1976) data for radial flow in a granite fracture, we used his results for both the loading and unloading cycles. Fig. 8 shows the

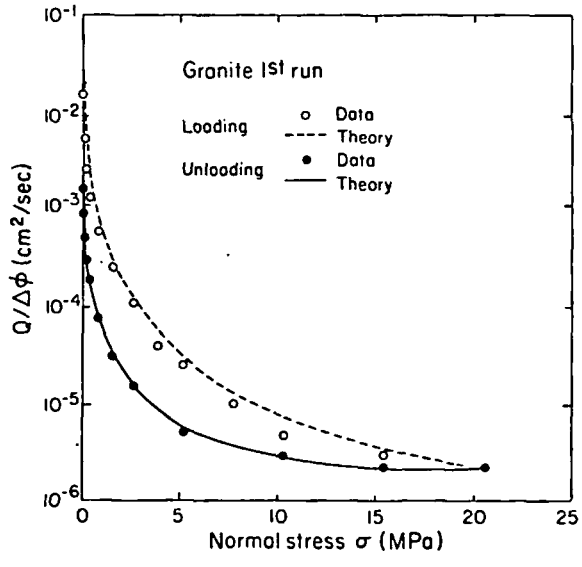

Fig. 8 Experimental and theoretical flow as a function of normal stress in the first loading and unloading cycles in granite.

hysteresis that he observed as a result of a permanent set in the fracture. We assumed a maximum fractional contact area of 15% at maximum applied stress and the smooth curves indicate how our theory compares with his experimental data. Since no curve fitting is involved in handling the flow data, we believe our theory probably contains the essential physics that is relevant to the coupling between stress and flow in a deforming fracture.

Summmary

Both a "void" and an "asperity" description of the fractures are used in this theory. The former is suited to the mechanical property, and the latter, to the hydrological property of the rough-walled fracture. The physical picture that emerges from such a model is that at zero applied stress, the fracture is propped open by only a few tall asperities, giving rise to very long average "crack" lengths. Therefore, the elastic property of the jointed rock appears to be extremely soft at low applied stresses. At higher stresses, the number of asperities in contact increases rapidly, causing a rapid decrease in the average crack length. Thus, the Young's modulus of the jointed rock approaches that of the intact rock.

The fact that the fractional contact area of the fracture at the maximum applied stress of 20 MPa is on the order of 0.15 is of considerable interest. While the stress-displacement measurements indicate that the Young's modulus of the jointed rock becomes almost identical to that of the intact rock at this stress level, the fracture is far from being "closed"; in fact, only about 15% of the fracture surfaces is in contact. The mechanical property of the fracture becomes indistinguishable from that of the intact rock, not because the fracture is "closed," but because the average crack length under increased load has shortened sufficiently, causing the voids in the fracture to deform from elongated shapes (Figs. 4 and 5) to voids more like spheroids. Thus, with respect to its elastic behavior, the fracture is very much like an intact rock; but with respect to its hydraulic behavior, the fracture is definitely "open" to allow fluid transport. Our observation therefore indicates that unless there are very high normal stresses, a fracture probably cannot be "closed" sufficiently to completely prevent hydraulic flow. This seems to be consistent with the observation of Kranz et al. (1979) from their measurement of permeability from pulse decay data. Kranz et al. deduced indirectly from their data that the difference in the flow rate between a jointed and an unjointed rock does not vanish until the effective pressure is at least 200-300 MPa.

POROUS MEDIA EQUIVALENT FOR A NETWORK OF DISCONTINUOUS FRACTURES

One of the important questions that arises when considering the flow of fluids through a discontinuous rock mass is whether or not the fracture network behaves like porous media. In other words, can one model the system by an equivalent permeability tensor and proceed to determine the movement of fluids under the application of known boundary and initial conditions?

Work that has been done to determine the equivalent permeability of fractured rocks from information on fracture geometry (assuming an impermeable matrix) can be classified into two categories. Most of the work that has been done falls into the first category where fractures are assumed to be of infinite extent (continuous or extensive fractures). Very little work has been done in the second category, taking into account the finite or nonextensive nature of fracture size.

Mathematical studies of extensive fracture systems were made by Snow (1965). Snow developed a mathematical expression for the permeability tensor of a single fracture of arbitrary orientation and aperture relative to a fixed coordinate system. The permeability tensor for a network of fractures is therefore the tensor formed by adding the respective components of the permeability tensors for each individual fracture.

It can be seen in the field that fractures are clearly of finite dimensions. The fact that fractures are finite means that each fracture can contribute to the permeability of the rock only insofar as it intersects other conducting fractures. In the extreme, an isolated fracture which does not intersect any other fracture effectively contributes nothing to the permeability of the total rock mass. This means that flow in any given fracture is not independent of flow in every other fracture.

Two approaches have been taken to account for the finite nature of real fractures. Parsons (1966) and Caldwell (1971, 1972) have used analogue models to study finite fractures. Rocha and Franciss (1977) have proposed a field method for finding a correction factor to Snow's (1965) analysis.

A significant result of Parson's work was that doubling the permeability of all fracture elements in the x direction increased the permeability in the y direction. This effect would not be seen in continuous fractures, but with discontinuous fractures the net flow in the y direction must proceed through some fractures oriented in the x direction. Also, for a similar reason, permeability in the x direction is less than doubled. This is a significant property of fracture systems that must be kept in mind.

Homogeneous Anistropic Permeability

In order to determine when a fractured medium behaves as a homogeneous, anistropic medium, one must determine if a symmetric permeability tensor exists. The only way to show this is to actually measure the directional permeability. Darcy's law:

$$q_i = K_{ij} \frac{\partial \phi_i}{\partial x_j} \qquad (13)$$

can be used to examine the theory of directional permeability measurement. The fact that flow and gradient are not necessarily in the same direction can be seen from inspection of the above Darcy equation. Only when flow and gradient coincide with one of the principle axes of permeability will flow and gradient be in the same direction.

Marcus and Evanson (1961), Marcus (1962), and Bear (1972) give both the expression for permeability in the direction of flow and permeability in the direction of gradient. Both show how the results of

directional permeability measurement can be plotted as ellipsoids. For K_f, the permeability measured in the direction of flux, $\sqrt{K_f}$ plotted versus α, the direction of measurement, on polar coordinate paper will be an ellipsoid given by:

$$1 = \frac{x^2}{K_1} + \frac{y^2}{K_2} + \frac{z^2}{K_3} \tag{14}$$

Likewise for K_g, the permeability in the direction of the gradient, $1/\sqrt{K_g}$ plotted versus α will be an ellipsoid given by:

$$1 = \frac{x^2}{1/K_1} + \frac{y^2}{1/K_2} + \frac{z^2}{1/K_3} \tag{15}$$

For permeability measured in the direction of flux, the major axis of the ellipsoid is in the direction of maximum permeability. For permeability measured in the direction of the gradient, the major axis of the ellipsoid is in the direction of minimum permeability.

Another basic problem is that of establishing homogeneity. Homogeneity has been discussed by Hubbert (1956), Fara and Scheidigger (1961), Toth (1967), Bear (1972), and Freeze (1975). Freeze points out that there is really no such thing as a truly homogeneous medium in geology. However, in order to have a tractable analysis of flow, a scale of measurement (the macroscopic scale) must be found for which the porous medium is seen as a continuum (Hubbert, 1956). On this scale the medium is said to be homogeneous. The scale at which analysis is possible is commonly illustrated with a diagram such as Figure 9. The volume at which the parameter

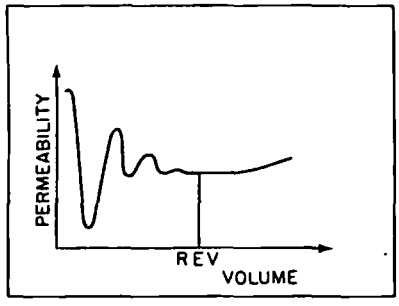

Fig. 9 Change in value of measured permeability with size of sample.

of interest, in this case permeability, ceases to vary is defined as the representative elementary volume (REV). With respect to permeability, the REV of a medium can be sought by measuring the average permeability of increasing volumes of rock until the value does not change significantly with the addition or subtraction of a small volume of rock.

There is no guarantee that such an REV exists for every permeable system. Indeed, Snow's (1969) theoretical and experimental work shows the permeability of fractured rock may continue to increase with the volume tested. This implies that the statistical sample continues to change with the size of the sample. A further problem has been studied by Freeze (1975), Smith and Freeze (1979a, 1979b), and Smith (1978). They have concluded that for some problems it may not always be possible to define equivalent homogeneous properties for inherently heterogeneous systems.

The difficulty in identifying equivalent permeability is that, (a) the equivalent permeability tensor that works for one set of boundary conditions will not necessarily predict the correct flux for another set of boundary conditions, and (b) an equivalent permeability which is correct in terms of flux may not predict the correct average head distribution. The first difficulty arises because, in general, different boundary conditions induce different gradients in different parts of the flow field. The permeability in one part of the field which has a higher gradient will have more effect on the total flux than the permeability in another part of the field which has a lower gradient. When the boundary conditions change, the emphasis changes. Therefore, a given equivalent permeability tensor will only apply absolutely to kinematically similar flow systems.

If the gradient within the internally heterogeneous REV remains approximately constant, each part of the element will have equal emphasis, and it may be possible to define a unique equivalent permeability tensor which will be correct for approximately linear flow in any direction. However, if the isopotentials and flow lines are curved relative to the dimensions of the statistically determined REV, then the value of the equivalent permeability of the REV will depend on the particular kinematics of the flow system. In this case, analysis of the flow system would depend on the knowledge of the equivalent permeability and the value of the equivalent permeability would depend on the flow system. So a unique solution to the flow problem is not guaranteed. If, on the other hand, the gradient is constant and the average flow lines are linear within the statistically determined REV, then there may exist a single permeability tensor which can be used to correctly predict flow in any direction. However, even under the constraints of a constant gradient, there is still no guarantee that a unique, symmetric permeability tensor will exist for every medium on any scale.

Given a flow system such as seepage under a dam, the size of the appropriate REV must be small enough to have approximately a constant gradient throughout and therefore linear average flow lines. However, it must also be large enough to contain a representative sample of the heterogeneities. In some cases, it may be that a statistically defined REV is too large to have linear average flow lines. In this case, either a smaller REV must be found as the basis for analysis or a non-continuum analysis must be used.

The above discussion leads to several conclusions central to this investigation. First, it only makes sense to look for REVs in fractured rocks using flow systems which would produce a constant gradient and linear flow lines in a truly homogeneous, anisotropic medium. Boundary conditions which produce such a flow system will be described below. Second, the following criteria must be met in order to replace a heterogeneous system of given dimensions with an equivalent homogeneous system for the purposes of analysis:

(1) there is an insignificant change in the value of the equivalent permeability with a small addition or subtraction to the flow volume;

(2) an equivalent symmetric permeability tensor exists which predicts the correct flux when the direction of gradient is changed.

Point (1) implies that the size of the sample under consideration is a good statistical sample of the heterogeneities. Point (2) implies that the boundary conditions are applied to the sample which would produce a constant gradient throughout a truly homogeneous anisotropic sample. The actual gradient within the heterogeneous sample does not have to be exactly constant for (2) to be satisfied.

Statistics of Fracture Geometry

Under a given set of boundary conditions, the hydraulic behavior of a fractured rock mass with an impermeable matrix is determined entirely by the geometry of the fracture system. Real fractures have complex surfaces and variable apertures, but for the purposes of this study and most other studies of fracture systems, the geometric description is simplified. The assumption is made that individual fractures lie in a single plane and have a constant hydraulic aperture. Characterization of a fracture system is considered complete when each fracture is described in terms of: (1) hydraulic or effective aperture, (2) orientation, (3) location, and (4) size.

As has been discussed in the first part of this review, the hydraulic behavior of fractures has been shown to be a function of their aperture (equation 11). Characterization of the permeability of a fracture requires determining the hydraulic aperture. Unfortunately, it is very difficult to perform hydraulic tests on isolated fractures in the field. For example, Gale (1975) isolated a limited number of horizontal fractures with packers and performed injection tests to determine their apertures. Gale's data, however, is not extensive enough to make significant analysis of the relationship between hydraulic and apparent apertures.

Because of the difficulty involved in hydraulically isolating a single fracture underground, what we know of fracture aperture distributions is limited to apparent apertures that have been observed directly in cores or well logs. The distribution of apertures measured by Bianchi and Snow (1968) was found to be very close to lognormal. It may be reasonable to expect the distribution of true hydraulic apertures to also be distributed lognormally.

The statistics of fracture orientation are perhaps the best understood of all the geometric properties of fractures. Orientation is easily measured in cores or in outcrops with simple tools. For instance, Mahtab (1972) developed a computerized method for analyzing clusters of orientation data. Once clusters had been identified they were compared to Arnold's hemispherical normal distribution.

The mathematical description of fracture locations and fracture dimensions are interrelated. Fracture traces can be observed in outcrops or in excavations. The location of the intersections of fractures within a borehole can also be determined. What we know about the location of fractures in space and their shape and dimensions comes from this trace length and intersection data.

Robertson (1970), Priest and Hudson (1976), Hudson and Priest (1979), and Baecher (1978) have studied length and spacing distributions for fractures. Baecher et al. (1977) have reviewed this literature on spacing and length distribution. Spacing and length have both been reported to vary exponentially and lognormally. Baecher (1978) developed a conceptual joint geometry model. Joint trace lengths are assumed to be lognormally distributed and spacings are assumed to be exponentially distributed. The authors infer that joints are circular disks randomly distributed in space. Joint radii are shown to be lognormally distributed.

Numerical Method of Analysis

A numerical code has been developed to generate sample fracture systems in two dimensions using the geometric properties described above and to determine the permeability of such systems. The computer program has been used to study samples of both extensive and nonextensive fracture networks.

The two-dimensional mesh generator produces random realizations of a population of fractures. Input to the generator includes specification of the distributions that describe the fracture population. The mesh generator can randomly choose fractures for the sample according to these distributions. Details of the scheme for mesh generation are given by Long et al. (1981). A finite element analysis can then be used to calculate Q_g, the component of flow through the pattern in the direction of the gradient. Using Darcy's law, the hydraulic conductivity in the direction of the gradient of the sample fracture pattern is calculated from:

$$K_g = \frac{Q_g}{A \nabla \phi} \tag{16}$$

where A is the gross area perpendicular to flow. The analysis of permeability is independent of the type of fracture model generated. This generator produces models similar to Baecher's (1978) but another fracture model, such as that proposed by Veneziano (1979) could just as easily have been used.

The effect of sample size on conductivity measurement can be studied with this program. First a large fracture pattern is generated. A small piece of this sample can be numerically removed and subjected to the numerical conductivity test described above (equation 16). Succeedingly larger pieces can be tested and the results compared.

The program can also be used to study the variation in conductivity between different realizations of a statistically described fracture system. This Monte Carlo type analysis could also be used to analyze statistical data collected in the field. An expected value and standard deviation of equivalent porous media conductivity would be obtained in this way.

As previously discussed, a method which obtains conductivity in the direction of the gradient must be used. Gradient can be approximately linear throughout a heterogeneous region in steady flow if the region is an REV. The direction of flow, however, is controlled by the direction of the fractures. The boundary conditions necessary to produce a constant gradient in a rectangular, anisotropic flow region are illustrated in Fig. 10. It consists of two constant-head boundaries (sides 2 and 4) and two boundaries (sides 1 and 3) with the same linear

variation in head from $\phi_2 = 1.0$ to $\phi_4 = 0$. An example of the configuration used in these analyses is shown in Fig. 10. Conductivity is measured in the direction perpendicular to sides 2 and 4.

The linearly varying boundary conditions on sides 1 and 3 are necessary because, in general, the medium in the flow region is anisotropic. Without these boundaries the lines of constant head would be distorted near sides 2 and 4.

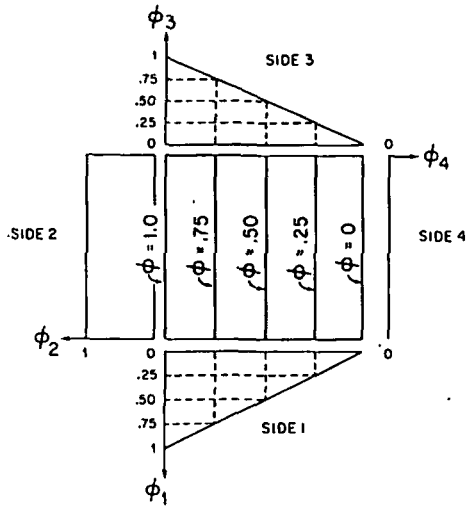

Fig. 10 Boundary conditions necessary to produce constant gradient in a homogeneous anisotropic flow region.

For the boundary conditions shown in Fig. 10, $\partial\phi/\partial y$ is zero. K_{xx} can be calculated from:

$$K_{xx} = \frac{\frac{Q_x}{(\phi_2 - \phi_4)L}}{L} = \frac{Q_x}{\phi_2 - \phi_4}. \qquad (17)$$

where Q_x is the total flux per unit thickness in the x direction. For $\phi_2 = 1$ and $\phi_4 = 0$, and consistent units, K_{xx} is numerically equal to Q_x. Also, since Q_y, the total flux per unit thickness in the y direction, is known, K_{xy} can be calculated from:

$$K_{xy} = \frac{\frac{Q_y}{(\phi_2 - \phi_4)L}}{L} = \frac{Q_y}{\phi_2 - \phi_4} \qquad (18)$$

For $\phi_2 = 1$ and $\phi_4 = 0$, as above, $K_{xy} = Q_y$.

Flow through the fracture system is computed using a finite-element program developed by Wilson and Witherspoon (1970) for fracture flow. Fractures are represented as line elements with flux related to aperture by the cubic law. The rock matrix is assumed to be impermeable. Only the steady state flow rate is calculated.

In general, the fracture pattern results in an anisotropic medium. Conductivity in such a fracture pattern can be measured in any direction chosen. For homogeneous anisotropic media, $1/\sqrt{K_{xx}}$ versus α, the angle of rotation, is an ellipse when plotted in polar coordinates. However, for inhomogeneous fractured media, $1/\sqrt{K_{xx}}$ may not plot as a smooth ellipse. In fact, the shape of a plot using measured values of K_{xx} for a given area of rock may be quite erratic. This plot can be used as a test of whether or not the given area can be approximated as a homogeneous porous medium. If $1/\sqrt{K_{xx}}$ does not plot at least approximately as an ellipse, then no single symmetric conductivity tensor can be written to describe the medium. If there is no conductivity tensor then flow through the medium cannot be analyzed by existing continuum techniques.

Validation of Numerical Method

The following two examples will illustrate the use of this numerical method of analyzing flow in two-dimensional networks of fractures. The first example is a fracture system of known conductivity and was used to verify the numerical method of permeability measurement. The conductivity of fracture systems with infinitely long fractures is known from the theory developed by Snow (1965) and others. Because of the physical basis of this fracture model, we could only examine finite pieces of such fracture systems. The infinite fractures are seen in a finite model as fractures which transect the entire model. An arbitrary extensive fracture system with two sets of parallel, evenly spaced, equal aperture fractures was tested. To provide an anisotropic case, the two sets were placed 30° apart. The numerical code was used to determine K_g for variations of α ranging from 0° to 105° as measured from one of the two fracture sets. Theoretically, this fracture network should produce an ellipse for $1/\sqrt{K_g}$ as shown by the solid line on the polar plot in Fig. 11. The plotted points represent the results

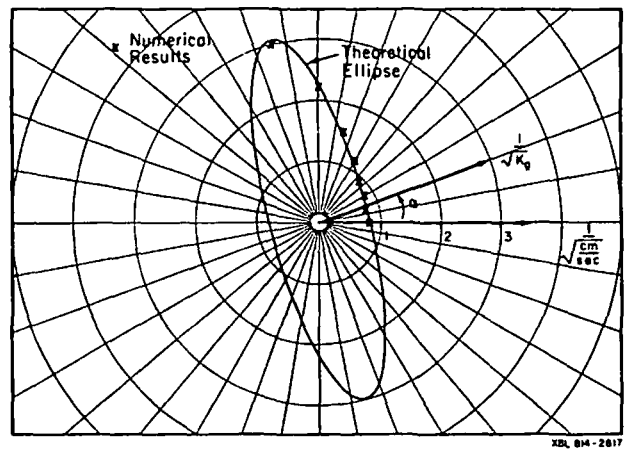

Fig. 11 Polar plot of numerical results for $1/\sqrt{K_g}$ compared to theoretical ellipse. Extensive fracture system composed of two sets of parallel, evenly spaced, equal aperture fractures placed 30° apart.

from the numerical analysis as the direction of the hydraulic gradient was changed in increments of 15°. The small differences between theoretical and numerical results can be attributed to the finite nature of the numerical model. Obviously, a fracture network with these properties could be replaced by an equivalent porous media.

The second example is a nonextensive fracture system that was developed at random using the mesh generation scheme described by Long et al. (1981).

Table 1 gives the statistics used to generate the fractures. The generation region was 110cm x 110cm.

Table 1. Input parameters for random network of fractures.

Parameters		Set 1	Set 2
Density	Number of Fractures	49	100
Orientation	Normal distribution m, s^2 (deg)	30, 5	60, 10
Length	Lognormal distribution m, s^2 (cm)	40, 10	30, 7.5
Aperture	Lognormal distribution m, s^2 (cm)	.001, .005	.005, .0001

To determine what variations might be expected from a repetitive generation of networks having the same parameters listed in Table 1, three different fracture systems were examined. Flow regions 75cm x 75cm oriented with $\alpha = 0°$ were investigated in each network. The three regions had network characteristics as given in Table 2.

Table 2. Characteristics of three random fracture networks.

Network	Number of Fractures	Number of Fracture Intersections	Number of Nodes	Number of Elements
1	81	123	285	327
2	86	110	282	306
3	90	139	319	368

Boundary conditions were applied to these three flow regions such that conductivity in the same direction could be measured. That is, sides 1 and 3 were given a linearly varying head distribution, side 2 had a constant head of 1, side 4 had a constant head of 0 (see Fig. 10). Table 3 gives the total fluxes in cm^3/s from each side for each flow region. A positive sign indicates flow into the region and a negative sign indicates flow out of the region.

Table 3. Total fluxes for three random fracture networks.

Network	Side 1 cm^3/s	Side 2 cm^3/s	Side 3 cm^3/s	Side 4 cm^3/s
1	0.13402E-19	4.41796E-7	-4.41384E-7	-4.11388E-10
2	0.39260E-10	2.00821E-5	-2.00809E-5	-8.67380E-10
3	0.42390E-10	1.01927E-4	-1.01927E-4	-8.97845E-11

Examination of Table 3 leads to several conclusions. First, there is a great deal of variation between the three networks generated using the same statistical fracture population. As shown in Table 2, the number of fractures in each flow region varies. Thus some of the variation in flow rate is due to nonergotic sampling. Recall that under the boundary conditions used, for an ideal porous medium the flux in the x direction, i.e. from side 2 to side 4, is numerically equal to the conductivity. However, examination of Table 3 shows that the flux into side 2 does not equal the flux out of side 4. The sum of the fluxes through all sides, however, is zero as expected. These samples are clearly not behaving like porous media. In anisotropic porous media under the chosen boundary conditions the flux on opposite sides would be equal.

To investigate the problem of directional permeability, Network 3 was selected for further analysis. Flow regions 75cm x 75cm in size were rotated at intervals of 15° so that α could be varied from 0° to 180°. Fig. 12A shows the fracture network of the

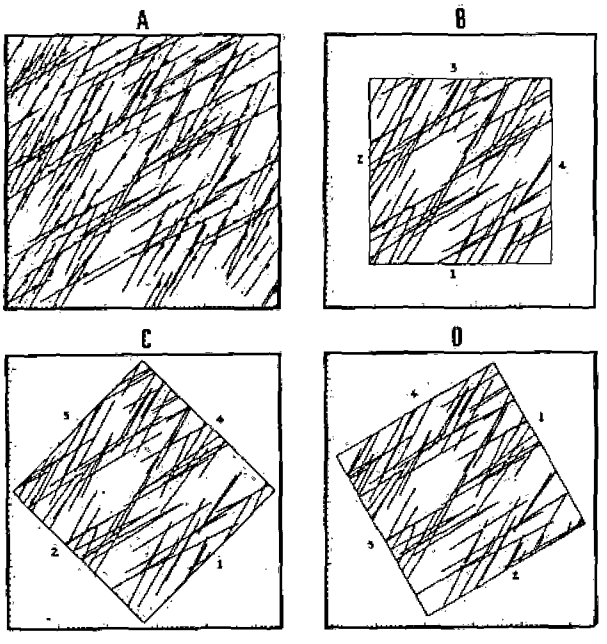

Fig. 12 Nonextensive random fracture system showing original generation region (A), and flow regions investigated when $\alpha = 0°$ (B), $\alpha = 45°$ (C), and $\alpha = 120°$ (D).

original generation region and Figs. 12B-C-D illustrate how different flow regions were created simply by rotating the boundaries while the network remained fixed.

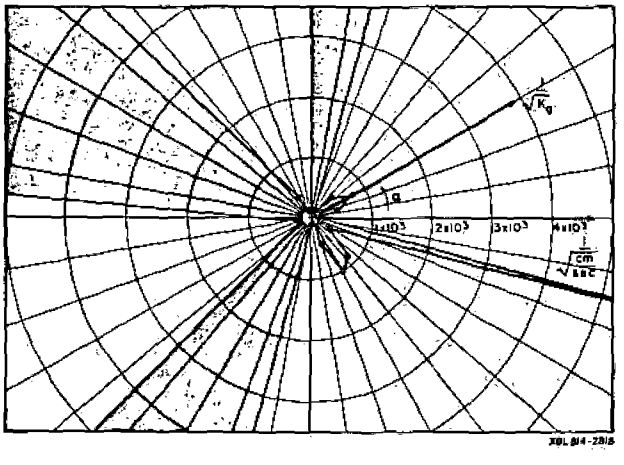

Fig. 13 Polar plot of numerical results for $1/\sqrt{K_g}$ for a nonextensive random fracture system.

Figure 13 shows the values of $1/\sqrt{K_g}$ plotted on polar coordinate paper where K_g is defined in terms of flux across side 2. The fact that inflow does not equal outflow on opposite sides leads to a problem in defining conductivity. If conductivity is arbitrarily defined as numerically equal to the inflow into side 2, no information is lost. Side 2 for any angle α becomes side 4 for $\alpha + 180°$, etc.

The results on Fig. 13 clearly do not plot as an ellipse; nor are they symmetric. For certain angles of rotation (e.g., 75°, 90°) the value of $1/\sqrt{K_g}$ becomes very large and goes off the scale of the graph. For these angles, K_g is very small because there is practically no hydraulic connection between sides 2 and any other side. This cannot be completely confirmed visually from the plots of these flow regions because aperture has not been included in the figures. Although isopotentials have not been plotted for these samples, it is fairly certain they will not be linear. If we define K_{yx} as numerically equal to the flow into or out of side 3, then K_{xy} is the flow into or out of side 1 when the flow mesh is rotated 90°. K_{xy} should equal K_{yx} if K_{ij} is symmetric. For this example, computed values of K_{yx} did not equal computed values of K_{xy} for any angle of rotation. This further demonstrates the nonsymmetric nature of the permeability.

The tests described above show clearly that the sample chosen does not have a symmetric conductivity tensor and cannot be represented by an equivalent porous medium. As further proof of the nonhomogeneous nature of Network 3, flow regions of different sizes were extracted and tested. The particular orientation shown on Fig. 12 for $\alpha = 0°$ was selected, and the flow region was reduced from 75cm x 75cm to 25cm x 25cm, while remaining centrally located in the original generation region. The results revealed order of magnitude changes in hydraulic conductivity from sample to sample and further illustrated the marked differences between the fluid flow behavior of this random fracture network and that of homogeneous porous media.

Summary

A numerical model has been developed to produce random networks of fractures. A computer program for fluid-flow analysis then measures the directional conductivity of these samples.

To determine if the fractured rock samples behave like porous media, the samples must be subjected to boundary conditions which would produce a constant gradient in homogeneous anisotropic media. If the medium has an equivalent porous medium permeability, these directional conductivity measurements should plot as an ellipse when $1/\sqrt{K_g}$ is plotted versus direction α on polar coordinate paper. Also, inflow will equal outflow on opposite sides of the rectangular volume element tested, and measured values of K_{xy} will equal measured values of K_{yx}. Average isopotentials within the element will probably be linear, but this is not a necessary criterion for behavior as an equivalent porous medium. If the volume of the element tested is changed slightly, the measured values of K_{ij} should not change significantly.

It is possible to find a fractured rock population for which no equivalent homogeneous porous medium permeability exists. This can occur for one of two reasons. First, the size of the REV may exceed the volume of rock that exists. Secondly, for the case of an impermeable matrix, the fractures may not be dense enough to behave as a medium with a symmetric permeability tensor. Non-"tensorial" behavior would result from insufficient interconnections between fractures. In this case, the volume of fractured rock may be large enough to be a good sample of the fracture population, but the nature of the fractures is such that they will not behave hydraulically as a porous medium on any scale.

The numerical techniques described here will be used to find fractured rock systems that do behave like anisotropic porous media. Fracture systems with specified geometries (spacing, aperture, length, and orientation) will be investigated. If the total number of fractures is held constant, the density of the fractures will be increased until systems are found which behave more like porous media. For a given population and a given total number of fractures, we should be able to identify minimum fracture densities which produce homogeneous anisotropic behavior. The effect of each distributed parameter on the size of the REV and the value of the resulting conductivity can then be determined.

Systems for which no REV exists will also be sought. This can be done by examining systems that are not dense enough to act like porous media. By holding this density constant and increasing the area of investigation, we can see if the behavior of the system becomes more like that of porous media or remains erratic.

Methods for quantifying the porous media nature of fracture systems are under development. One method currently being investigated is to quantify how well the permeability data plot as an ellipse. Such an approach should lead to an understanding of the errors that can result from assuming a porous medium equivalent for a fractured rock mass when no such equivalence exists. Ultimately, our goal is to be able to analyze field data on fracture systems to determine when it is appropriate to make the simplifying assumption of a porous medium equivalent. This, of course, will require an understanding of the need to extend the technique to three dimensions.

COUPLED THERMAL-HYDRAULIC-MECHANICAL FINITE ELEMENT MODEL FOR SATURATED FRACTURED POROUS MEDIA

In the usual treatment of fluid flow in porous media, the rock deformation has been considered through the concept of the coefficient of specific storage. This approach, although by no means precise, is adequate to represent most fluid flow problems. A more realistic treatment of the fluid flow behavior of deformable porous media came about after the introduction of the well-known theory of consolidation by Terzaghi (1925). With the advent of computers, numerical solution techniques for coupled one-dimensional equations of consolidation and multidimensional equations of fluid flow provided an approximate means of analyzing general fluid flow problems in deformable porous media (Helm, 1974, Narasimhan and Witherspoon 1977). Biot (1940) introduced the general theory of consolidation which makes possible a more realistic treatment of the hydromechanical behavior of saturated porous rocks. In an attempt to develop a method for the solution of general consolidation problems, Sandhu and Wilson (1969) applied the variational finite element method

to the problem of fluid flow through saturated porous elastic solids. This method was extended by Ghaboussi and Wilson (1971) in considering effects of fluid compressibility.

The theories of mixtures (Green and Naghdi, 1965), Crochet and Naghdi (1966), which have a sound thermodynamical basis and a general associated constitutive theory, can be reduced to a special case of a theory for flow of fluids through porous elastic solids which is equivalent to Biot's work. The basic assumption of this approach leads to certain conceptual difficulties in the physical interpretation of partial stresses.

Recently Safai and Pinder (1979), in a Galerkin finite element method of analysis for fluid flow through deformable porous media, made an attempt to consider the entire saturated-unsaturated flow regime. The proper constitutive stress-strain relationship for the extension of Biot's (1940) theory to the entire flow regime was later provided by Noorishad et al (1981a).

Consideration of fracture deformability along with its hydromechanical behavior has appeared in the literature mainly since 1965. Davis and Moore (1965) measured one of the first direct evidences of fracture deformations of the order of microns caused by earth tides. Snow (1968) reported strains of 10^{-7} to 10^{-8} at a distance of about 300 ft from a water well in metamorphic rocks subjected to a significant drawdown. To handle this behavior, the early hydraulic and hydromechanical analysis of fractures was achieved using an equivalent porous medium approach. Theoretical and numerical studies of fluid flow in a rock mass taking into account the deformable nature of fractures in a discrete manner was first carried out by Noorishad et al. (1971). This work was based on earlier studies of discrete fracture behavior from a load-deformation point of view by Goodman et al. (1968) and a fluid flow point of view by Wilson and Witherspoon (1970).

Numerical studies on deformable fractured rocks have been carried out by Rodatz and Wittke (1972) and Gale (1975). Iwai (1976) made a detailed series of laboratory tests on flow through a single fracture under load. The laboratory and field tests by Gale (1975) provided strong evidence of a nonlinear fracture deformability induced by fluid pressure changes and also verified the capability of the numerical solution technique. The static approach of Noorishad et al (1971) was later extended by Hilber et al. (1979) into the dynamic range where stick-slip phenomena due to injection of an incompressible fluid in a nonporous fractured rock was studied.

A two-medium statistical-numerical model was presented by Duguid (1973) who extended the method introduced by Barenblatt et al (1960) to fissured elastic porous media using a finite element numerical procedure. A deterministic solution for transient flow of fluids in deformable fractured porous rocks was recently achieved using an enumerative approach (Ayatollahi, 1978). This variational finite element technique is based on a generalization of Biot's (1940) constitutive stress-strain equation and uses a Gurtin (1964) type variational principal. An extension of this work by Noorishad et al. (1981b) provides a general two-dimensional, finite element solution technique for the investigation of the deformation, stress distribution, fluid storage, and fluid flow properties of a fractured porous medium under the influence of hydraulic and structural boundary conditions. At present, several groups are investigating a host of numerical hydromechanical models which are at different stages of development. Baca (1980) and Tsang (1980) have summarized the capabilities of some of these new models.

The presence of heat in fluid flow regimes brings about a chain of coupled effects which shall be referred to here as thermal-hydraulic-mechanical phenomena. The coupled phenomena for fluid and heat flow, usually known as hydrothermal flow, have been the subject of several detailed studies. A complete account of the state-of-the-art can be found in Pinder (1979) and Wang et al (1980). However, it should be pointed out that hydrothermal investigation of discontinuous rock masses is a problem that needs much more investigation.

Studies of thermal effects on linear and nonlinear materials, known as thermoelasticity, are thoroughly covered in the physics and engineering disciplines and need not be considered here. As far as rock mechanics usage is concerned, thermoelasticity lies mostly within the confines of continuum applications. An account of the status and needs of the thermomechanical modeling techniques for continuous and discontinuous media is given by Hocking (1979). More recent reports (Bacca, 1980; Tsang, 1980) indicate that a number of the new, developing models either have provisions for incorporating fractures or actually have the capability of modeling the discontinuities in a discrete manner.

A natural outgrowth of hydromechanical, hydrothermal, and thermomechanical modeling techniques is the development of a general model incorporating all of the above techniques. Baca (1980) and Wang et al. (1980) have reported that a number of research organizations are engaged in the development of such general modeling techniques but to our knowledge, the details have not yet been published. Various rock-water interaction studies have been underway in this laboratory for some years, and the development of an approach to the thermal-hydraulic-mechanical behavior (or hydrothermoelasticity) of fractured rocks is part of an ongoing effort (Noorishad and Witherspoon, 1981). The essential features of this coupled finite element method of analyzing fractured porous rocks will be presented below.

Field Equations

Using τ_{ij} for the components of the bulk stress tensor, P for fluid pressure, and T for temperature, Noorishad and Witherspoon (1981) have shown that the stress-strain relationship for an elastic isotropic porous medium can be written:

$$\tau_{ij} = 2\mu e_{ij} + \lambda\delta_{ij}\,\delta_{k\ell}e_{k\ell} - \beta\delta_{ij}T + \alpha\delta_{ij}P \qquad (19)$$

$$\xi = \frac{\rho_\ell}{\rho_o}\,\alpha\delta_{ij}e_{ij} + \frac{1}{M}\,P + \frac{1}{M_T}\,T$$

In the above equations the dependent variables e, T, and P are incremental in value and represent deviations from the zero state (stress-free state). Also, contact equilibrium between the fluid and the solid is assumed.

The governing equation for the fluid flow is written as:

$$\frac{\partial \xi}{\partial t} = \nabla \cdot \left[\frac{\rho_\ell \underline{k}_f}{\rho_o} (\nabla p + \rho_\ell g \nabla z) \right] \tag{20}$$

and ρ_ℓ and ρ_o are related through the equation of state for the fluid:

$$\rho_\ell = \rho_o \left[1 + \beta_T T + \beta_p P \right] \tag{21}$$

Note that internal or boundary source terms are absent in (20), a restriction which is later easily relaxed.

The law governing the static equilibrium is given as:

$$\frac{\partial \tau_{ij}}{\partial x_j} + \rho_s f_i = 0 \tag{22}$$

Finally the law for conservation of energy is represented in the following form:

$$\frac{\partial}{\partial t}[(\rho C)_M T + T_o \beta \delta_{ij} e_{ij}] + \varepsilon \rho_\ell C_{v\ell} \underline{q} \cdot \nabla T = \nabla \cdot \underline{K}_M \nabla T \tag{23}$$

where:

$$(\rho C)_M = \varepsilon \rho_\ell C_{v\ell} + (1 - \varepsilon) \rho_s C_{vs}$$

$$\underline{K}_M = \varepsilon \underline{K}_\ell + (1 - \varepsilon) \underline{K}_s$$

The Darcy fluid velocity $\underline{q}$ is given as:

$$\underline{q} = - \frac{\underline{k}_f}{\eta_\ell} (\nabla p + \rho_\ell g \nabla z) \tag{24}$$

The quantity T_o represents the absolute temperature in the stress-free state. In deriving the governing equation for heat flow (23), the following assumptions are made:

(i) thermal contact equilibrium between the fluid and the solid
(ii) energy associated with the fluid dilatation is negligible
(iii) fluid shearing stresses are absent in macroscopic sense
(iv) internal source terms and boundary source terms are absent.

The last assumption is later removed in the numerical algorithm.

The fundamental laws governing static equilibrium, fluid flow, and heat flow are coupled through the dependent variables of the solid displacement vector, fluid pressure, and macroscopic medium temperature. These laws, presented in equations 20, 22, and 23, in conjunction with constitutive equations 19 and 21 provide the complete mathematics of the coupled quasi-linear, thermal-hydraulic-mechanical phenomena in saturated porous elastic media. Extension of the above development to the nonlinear range is no major task and has already been accomplished. For the sake of simplicity, the extended development for the nonlinear fractured media will not be presented here. The above equations with proper initial and boundary conditions (see Appendix) define the mixed initial-boundary-value problem for thermal-hydraulic-mechanical phenomena in porous media.

Method of Solution

The complexity of the hydrothermoelasticity equations is such that an analytic (mathematical) solution for even simple initial and boundary value problems is not likely to be found. However, numerical solutions to the most general problems can easily be sought. Various numerical schemes using well-known numerical techniques, such as finite element and finite difference, can be utilized. In this work a finite element technique, was given strong preference because of earlier experience with this approach to linear and nonlinear problems of hydroelasticity (Ayatollahi, 1978; Noorishad et al., 1981b). A mixed variational and Galerkin finite element method forms the basis of this approach. As a result, the following set of matrix equations is obtained:

$$\underline{K}\,\underline{U} + \underline{C}_{UP}\underline{P} + \underline{C}_{UT}\underline{T} = \underline{F} \tag{25}$$

$$\underline{C}_{PU}\underline{U} + (\underline{E}_f + 1^*\underline{H}_f)\underline{P} + \underline{C}_{PT}\underline{T} = -1^*\underline{Q}_\ell \tag{26}$$

$$\underline{C}_{TU}\underline{U} + [\underline{E}_h + 1^*(\underline{H}_{hf} + \underline{H}_h)]\underline{T} = -1^*\underline{Q}_h \tag{27}$$

where 1^* represents time integration. Details of the method of solution and the complete expressions for the matrix coefficients are given in the Appendix.

To handle discretization in the time domain, two different schemes of time integration are used to integrate matrix equations 25, 26, and 27. A predictor-corrector scheme (Taylor, 1974) is used for the integration of the first two implicitly coupled equations (Ayatollahi et al., 1981). The energy equation uses a Crank-Nicholson step-by-step procedure with the solution of each time step being sought in the middle of the interval.

The coupling of (27) to (26) is nonlinear and is implicitly expressed in $\underline{H}_{hf}$, the nonsymmetric convective thermal conductivity matrix. The large time constant for the energy equation as compared to that of the flow equation suggests that the above formulation is easily adapted to an interlacing scheme of solutions such as used by Sorey (1975). This interlacing scheme uses the fluid velocities obtained from a direct solution of (25) and (26) and feeds back the temperature resulting from a solution of (27). This approach of explicitly solving the coupled equations is enhanced by the low sensitivity of the dependent variables P and U within some ranges of temperature in different problems. Therefore, the energy equation in these ranges can march through time using large time steps compared to the small time steps required to solve the other two equations. A further advantage is gained in situations where the mass transfer contribution to temperature distribution is negligible. In these cases a single solution for the energy equation provides the needed temperature information for the stepwise solution of the other two equations.

Three types of elements are used in this coupled technique: (a) two-dimensional isoparametric elements for solid fluid mixtures, (b) one-dimensional elements representing fracture segments from the flow point of view, and (c) one-dimensional joint elements to represent fracture segments for structural considerations. Natural coordinates are used for discretization of the displacement, pressure, and temperature

fields within the quadrilateral element. This leads to a parametric formulation for the corresponding integrals in terms of coordinate parameters for the porous solid-fluid mixture elements. Numerical integration is performed using the Gauss quadrature formula. The isoparametric bilinear function used for discretization and the parametric details can be found in finite element texts (Zienkiewicz, 1971]. For the structural joint element and the flow-line element, discretization of the displacement and pressure fields, is written in terms of local coordinates. Where necessary, the results are transformed to the global coordinate system. The assumption of uniform aperture within each fracture was used throughout the derivation of the matrices involving fracture volume integrals.

Validation of Numerical Scheme

The complexity of the coupled phenomena under consideration makes it possible to present only a partial verification of the method of analysis presented here. In the following discussion, we shall include results of the application of the method to hydromechanical, thermomechanical, and hydrothermal problems. These examples do not fully reveal the power of this approach.

In choosing an example of a hydromechanical problem, we examined a fracture flow problem for which an analytical solution exists (Raghavan et al., 1976). Since this problem does not require coupling between fluid flow and rock deformation, the coupling coefficient α was set to zero and 1/M was changed to S_s in equation 19.

The problem is that of a single vertical fracture intersecting a well of zero radius in a rectangular porous medium. The fracture is assumed to be rigid and of very high conductivity. The material properties of the fluid and rock are given in Table 4. Fig. 14 shows the finite element mesh used and Fig. 15 shows how the numerical results compare with the analytical solution (Raghavan et al., 1976). For the case $X_D = 1$, there is excellent agreement over the whole time span. In the case $X_D = 3$, the differences noted on Fig. 15 between numerical and analytical solutions is attributed to the coarseness of the finite element mesh. The half slope of the curve for P_D versus t_D at early time is often used as evidence in the petroleum literature for the presence of a fractured system (Gringarten et al., 1975).

This problem was also solved in a coupled manner where deformability in both the fracture and the matrix were introduced (Table 4). The fracture was also given a specific aperture (10^{-4}m) so that it had a finite permeability. The effect of treating

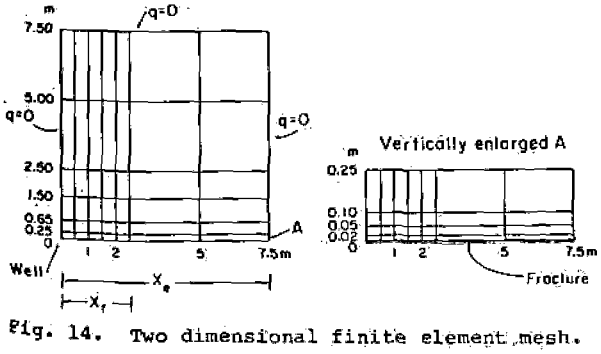

Fig. 14. Two dimensional finite element mesh.

Table 4. Material properties for hydromechanical analysis of fractured rock mass.

Material	Property	Value
Fluid	Mass density, ρ_ℓ	9.80×10^2 kg/m^3
	Compressibility, β_p	5.13×10^{-1} GPa^{-1}
	Dynamic viscosity, η_ℓ	2.80×10^{-4} N sec/m^2
Rock	Young's modulus, E_s	2.45 GPa
	Poisson's ratio, ν_s	0.25
	Mass density, ρ_s	2.5×10^3 kg/m^3
	Porosity, ϵ	0.15
	Intrinsic Permeability, k_f	10^{-12} m^2
	Biot's constant, M	1.47GPa, 14.0 GPa*
	Biot's coupling constant, α	1.0, 0.0*
Fractures	Initial normal stiffness, K_{fn}	1.60 GPa/m
	Initial tangential stiffness, K_{fs}	0.50 GPa/m
	Cohesion, C_o	0.0
	Friction angle, δ	30°
	Initial aperture, b	10^{-3}m, 10^{-4}m
	Porosity, ϵ	0.15
	Biot's constant, M	1.47 GPa, 14.0 GPa*
	Biot's constant, α	1.0,0.0*

*Used in the uncoupled case.

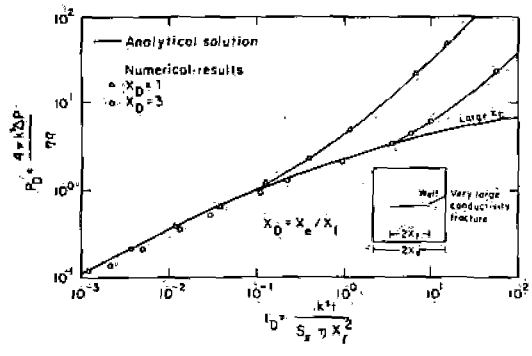

Fig. 15 P_D versus t_D for single vertical fracture of very large conductivity in porous medium. Analytical solution after Raghavan et al. (1976).

the system in this fashion is to change the pressure drawdowns significantly. For example, Fig. 16 shows how pressures decrease from the wellbore to the end of the vertical fracture. It will be noted that the pressure drop at the end of the fracture is about half that at the wellbore. For comparison, the problem was rerun in a decoupled mode and the pressure differences are far less (see curve labeled "fluid flow analysis" on Fig. 16).

Fig. 17 shows a plot of P_D versus t_D for this finite conductivity fracture problem to demonstrate the differences from the case of a very high conductivity fracture (Fig. 15). Note that at early time, the half slope relationship no longer holds. Note also the separation between the two curves that increases with time revealing the importance of fracture deformability and the need for coupled analysis.

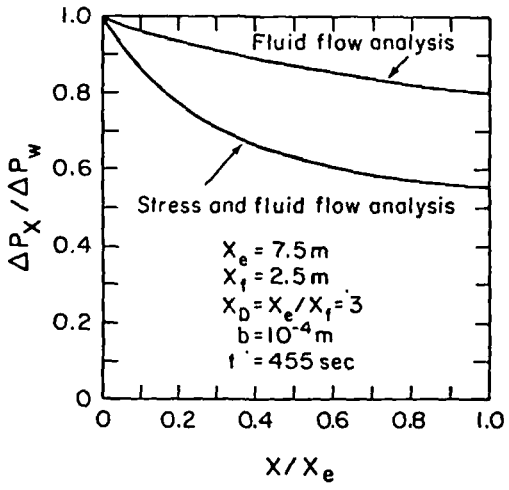

Fig. 16 Pressure drops along vertical fracture of finite conductivity in porous medium showing differences between analyses based only on fluid or on coupled stress and fluid flow.

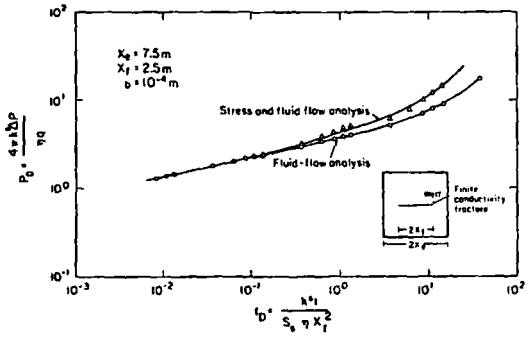

Fig. 17 P_D versus t_D for single fracture of finite conductivity in porous medium showing differences between analyses based only on fluid flow or on coupled stress and fluid flow.

In choosing a problem for a thermomechanical investigation, we first carried out some preliminary validation studies using both SAP4 and the present code. Solutions to two linear-elastic problems involving: (1) a finite line source in an infinite medium, and (2) a semi-infinite space subject to a constant temperature boundary condition were obtained. The results from the two approaches were in excellent agreement.

To demonstrate the ability of the code to handle non-linearities, a simple thermomechanical problem

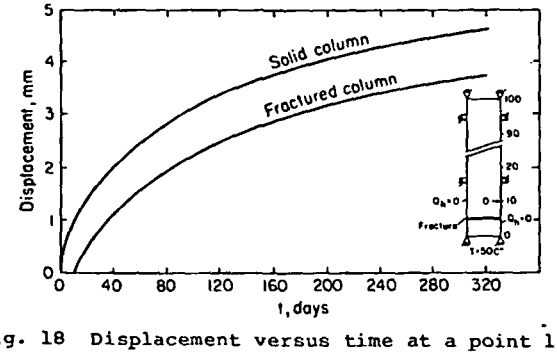

Fig. 18 Displacement versus time at a point 10m above base of rock column showing effect of fracture in reducing movement.

consisting of a long column of rock intersected near its base by a fracture was chosen (see inset on Fig. 18). Initially, the column temperature is 0°C, and after a step increase of 50° at the base, the problem is to determine the time variation of displacements above the fracture at a height of 10m. The material properties of the rock are given in Table 5. Fig. 18 shows the highly non-linear mechanical behavior of the fractured column and illustrates the ability of this finite element method to model discontinuous rock systems.

Table 5. Material properties for thermomechanical analysis of fractured rock column.

Property	Value
Mass density, ρ_s	2.5×10^3 kg/m^3
Specific heat capacity, C_{vs}	2.1×10^{-1} Kcal/kg °C
Thermal conductivity, K_s	7.65×10^{-4} Kcal/m sec °C
Thermal expansion coefficient, γ	1.11×10^{-5} °C^{-1}
Initial normal stiffness, K_{fn}	2.5×10^{-3} Pa/m
Young's modulus, E_s	5.13 MPa
Poisson's ratio, ν_s	0.25

An interesting problem that demonstrates only part of the hydrothermal capabilities of this code is the simulation of a saturated porous medium that is given a momentary thermal front. The onset of convective motion due to buoyancy is to be determined. The physical system consists of two porous reservoirs that initially are kept at temperatures T_o and T_1, as illustrated by the inset on Fig. 19. Initially, a thermal barrier separates the two reservoirs, both of which are horizontally semi-infinite and insulated top and bottom. At t = 0, the barrier is removed, and the problem is to determine the instantaneous horizontal velocity profile along the thermal front. An analytical solution for this problem has been published by Cleasson (1979).

This particular problem is very sensitive to the finite element mesh that is selected, and some effort was required to achieve the optimum grid for a specific number of nodal points. The problem was solved with a network of 252 elements requiring 286 nodal points. The material properties of the fluid and porous medium are given in Table 6.

Table 6. Material properties for hydrothermal analysis of thermal front problem.

Property	Value
Downstream temperature, T_o	20°C
Downstream mass density, ρ_o	9.98×10^2 kg/m^3
Downstream dynamic viscosity, η_o	9.89×10^{-4} kg/m sec
Upstream temperature, T_1	90°C
Upstream mass density, ρ_1	9.66×10^2 kg/m^3
Upstream dynamic viscosity, η_1	2.17×10^{-4} kg/m sec
Fluid thermal expansion coefficient, β_T	-4.46×10^{-4} °C^{-1}
Intrinsic permeability, k_f	10^{-12} m^2
Gravity acceleration, g	9.80 m/sec^2
$\frac{k_f(\rho_o-\rho_1)g}{\eta_o+\eta_1}$, q_o	2.42×10^{-7} m/sec
Finite element mesh width, W	900 m
Finite element mesh height, H	20 m

Fig. 19 shows a comparison of the numerical results for the instantaneous normal (horizontal)

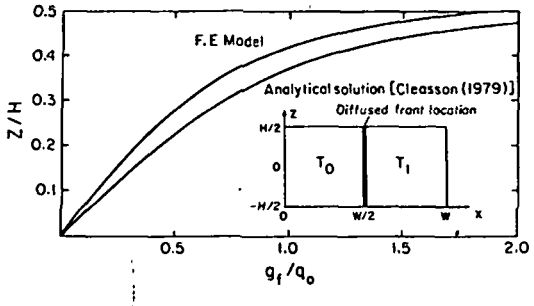

Fig. 19 Profile of instantaneous horizontal velocities due to buoyancy effects at location of thermal front in saturated porous media.

velocities compared with those of the analytical solution of Cleasson (1979). Considering the fact that in the numerical approach, the thermal front must be modelled by a zone of finite width, which in our case was 0.4m, the agreement is quite good. Further mesh refinement would undoubtedly lead to closer agreement with the analytical solution.

Summary

An extension of Biot's (1940) theory of consolidation is proposed here to provide a new technique for a realistic method of investigating the thermal-hydraulic-mechanical behavior of fractured porous media. A direct solution process has been developed that involves a variational formulation and a Galerkin integral to produce a set of three matrix equations. In this approach the equations of static equilibrium and fluid flow appear in an implicitly coupled form and the energy equation is explicitly coupled to these equations. Finite element descretization, along with two schemes for time descretization, yield the final form of the matrix equations which are then soved in a two-step procedure, referred to as an interlacing scheme.

A partial validation of this new technique is presented by considering applications to hydromechanical, thermomechanical, and hydrothermal problems. The hydromechanical problem involves the calculation of pressure drops in a vertical fracture that intersects a well and acts as a drain for the surrounding porous medium. The results reveal the errors that can occur when the interaction between hydraulic and mechanical stresses is ignored. The thermomechanical problem involves the calculation of the expansion of a rock column with a heat source placed at one end. When a fracture exists between the location of the heat source and a point where one is attempting to predict the magnitude of thermally induced displacements, a highly non-linear behavior results that will not be predicted if one ignores the existence of the discontinuity. The hydrothermal problem involves a saturated porous medium that is given a momentary thermal front. The difficulty in predicting the onset of a natural convective motion can be handled by this new technique when the appropriate finite element mesh is selected. Complete validation of this new thermal-hydraulic-mechanical finite element model for saturated fracturd porous media will require much more work.

ACKNOWLEDGEMENTS

This work was supported by the Director, Office of Energy Research, Office of Basic Energy Sciences, Division of Engineering, Mathematics, and Geosciences; and by the Assistant Secretary for Nuclear Energy, Office of Waste Isolation of the U. S. Department of Energy under Contract No. W-7405-ENG-48.

NOMENCLATURE

a	typical asperity size
A	fracture cross sectional area
A_1, A_2	structural boundaries where displacements and surface tractions are prescribed
b	fracture aperture
b_o	maximum fracture aperture
B_1, B_2 & C_1, C_2	fluid flow and heat flow boundary parts where Dirichlet or Neuman boundary conditions are prescribed
$\underline{C}$	elasticity matrix
C_{ijkl}	components of elasticity tensor for solid phase
C_o	fracture cohesion
$\underline{C}_{PT}$	pressure-temperature coupling matrix
$\underline{C}_{UP}$	displacement-pressure coupling matrix
$\underline{C}_{UT}$	displacement-temperature coupling matrix
C_{vl}	specific heat capacity of liquid at constant volume
C_{vs}	specific heat capacity of solid at constant volume
d	half-crack length
D/D^St	comoving time derivative following solid
e_{ij}	components of strain tensor for solid phase
E, E_s	Young's modulus for rock
E_{eff}	Effective Young's modulus for jointed rock
$\underline{E}_f$	fluid storativity matrix
$\underline{E}_h$	heat capacity matrix
f_i	components of body force vector
$\underline{F}$	force vector
g	gravitational acceleration
$\underline{G}$	traction vector on A_2 boundary
h	asperity height in fracture
$\underline{H}_f$	fluid conductivity matrix
$\underline{H}_h$	heat conductivity matrix
$\underline{H}_{hf}$	mass transfer conductivity matrix
$\underline{k}_f$	intrinsic permeability tensor
$\underline{K}$	stiffness matrix
K_{fn}	normal stiffness
K_{fs}	tangential stiffness
K_{ij}	permeability tensor components
K_f	permeability measured in the direction of flux
K_g	permeability measured in the direction of hydraulic gradient

$\underline{K}_\ell$	liquid thermal conductivity tensor
$\underline{K}_M$	solid-fluid mixture thermal conductivity tensor
$\underline{K}_s$	solid thermal conductivity tensor
$\underline{\ell}$	length of cylindrical rock sample
L	length of the boundary
m	distribution mean
M	Biot's constant for $1/\varepsilon\beta_p$
M_T	Biot's constant for $1/\varepsilon\beta_T$
M_v	number of voids in schematic representation of fracture
N	total number of elements in finite element idealization
$\underline{n}$	outward normal direction cosine vector
n_i	indices used to designate number of elements, i = 1, 2, 3
n(h)	asperity height distribution function
$N_c(\Delta V)$	number of areas of contact in fracture
P	pressure
$\hat{P}$	pressure assigned on B_1 boundary
$\underline{P}$	pressure vector
$\underline{P}_t$	pressure vector at preceding time step
ΔP_w	pressure drop
$\underline{q}$	fluid flow vector
q_i	components of fluid flow vector and the
q_f	horizontal component of fluid flow vector
q	rate of fluid discharge from well
Q	flow per unit width
Q_g	flow per unit width in direction of hydraulic gradient
$\underline{Q}_h$	heat flow vector
$\hat{Q}_h$	normal heat outflow from C_2 boundary
$\underline{Q}_\ell$	fluid flow vector
$\hat{Q}_\ell$	normal fluid outflow from B_2 boundary
s	distribution variance
S_s	specific storage coefficient of saturated porous elastic solid
T	temperature
$\underline{T}$	temperature vector
$\underline{T}_t$	temperature vector at preceding time step
u	volume enclosing one crack
$\underline{U}$	solid element displacement vector
V	space occupied by fluid-solid mixture
V^n	region of space occupied by fluid-solid mixture of an element n
ΔV	fracture deformation
ΔV_r	rock deformation
ΔV_t	total jointed rock deformation
x_i or x,y,z	Cartesian coordinates, i = 1,2,3
α	Biot's hydroelastic coupling coefficient or angle of orientation of hydraulic gradient
β	Thermoelastic coupling coefficient equal to $(2\mu+3\lambda)\gamma$
β_p	fluid compressibility
β_T	fluid thermal expansion coefficient
γ	solid thermal expansion coefficient
δ_{ij}	Kronecker delta function
δ	friction angle
ε	porosity
η_ℓ, η	liquid dynamic viscosity
λ	Lamé's elasticity constant
μ	Lamé's elasticity constant
ν	functional perturbation parameter
ν_s	Poisson's ratio
ξ	fluid volume strain
ρ_ℓ, $\hat{\rho}_\ell$	liquid mass density and average liquid mass density
ρ_s, $\hat{\rho}_s$	solid mass density and average solid mass density of porous space
ρ_M	solid-fluid mixture mass density
$(\rho C)_M$	solid-fluid heat capacity
$\underline{\tau}, \tau_{ij}$	stress tensor and components
$\underline{\tau}_T, \tau_{Tij}$	thermal stress tensor and components
τ, σ	stress normal to fracture
ϕ	hydraulic potential
$\underline{\Phi}_u$	displacement interpolation function matrix
$\underline{\Phi}_e$	strain-nodal displacement transformation matrix
$\underline{\Psi}$	pressure and temperature interpolation function matrix
$\underline{\Phi}_\theta$	transformation matrix for pressure or temperature gradients
ω	fractional fracture contact area

REFERENCES

AYATOLLAHI, M.S., 1978, Stress and Flow in Fractured Porous Media, Ph.D. Thesis, University of California, Berkeley.

AYATOLLAHI, M.S., J. NOORISHAD AND P. A. WITHERSPOON, 1981, A finite-element method for stress and fluid flow analysis in fractured rock masses, submitted to Journal of Engineering Mechanics Div., ASCE.

BACA, R.G., 1980, Coupled geomechanical/hydrological modeling: An overview of BWIP studies, in Proceedings ONWI Workshop on Thermomechanical-Hydrochemical Modeling for a Hard Rock Waste Repository, Berkeley, California, Lawrence Berkeley Laboratory Report LBL-11204, ONWI-164.

BAECHER, G.B., N.A. LANNEY AND H.H. EINSTEIN, 1977, Statistical descriptions of rock properties and sampling, Proceedings 18th U.S. Symposium on Rock Mechanics.

BAECHER, G.B., 1978, Trace length biases in joint surveys, Proceedings 19th U.S. Symposium on Rock Mechanics.

BARENBLATT, G., U.P. ZHELTOV AND G.H. KOCHINA, 1960, Basic concepts in the theory of seepage of homogeneous liquids in fractured rocks, in Prikladnaya Matem, i Mekh., v. 24, pp. 852-864, (in Russian).

BEAR, J., 1972, Dynamics of Fluids in Porous Media, American Elsevier Co., New York, London, Amsterdam.

BIANCHI, L. AND D.T. SNOW, 1968, Permeability of crystalline rock interpreted from measured orientations and apertures of fractures. Annals of the Arid Zone, v. 8, no. 2, pp. 231-245.

BIOT, M.A., 1940, General theory of three-dimensional consolidation, Journal Applied Physics, v. 12, pp. 155-164.

BOUSSINESQ, J., 1868, Journal de Liouville, v. 13, pp. 377-424.

CALDWELL, J.A., 1971, The Theoretical Determination of the Fluid Potential Distribution in Jointed Rocks, M.Sc. Thesis, University of Witwatersrand, Johannesburg, South Africa.

CALDWELL, J.A., 1972, The theoretical determination of the permeability tensor for jointed rock, Proceedings of Symposium on Percolation Through Fissured Rock, Stuttgart, 1972, Int'l. Soc. for Rock Mech. and Int'l Assoc. of Engineering Geology.

CLEASSON, J., 1979, Notes on Ground Water Thermohydraulics, Report, Dept. of Mathematical Physics, Lund, Sweden.

CROCHET, M.J. AND P.M. NAGHDI, 1966, On constitutive equations for flow of fluid through an elastic solid, International Journal of Engineering Science, v. 4, pp. 383-401.

DAVIS, S.N. AND G.W. MOORE, 1965, Semidiurnal movement along a bedrock joint in Wool Hollow Cave, California, National Speological Society Bulletin, v. 27, no. 4, pp. 133-142.

DUGUID, J.O., 1973, Flow in Fractured Porous Media, Ph.D. Thesis, Princeton University.

FARA, H.D. AND A.E. SCHEIDEGGER, 1961, Statistical geometry of porous media, Journal Geophysical Research. v. 66, pp. 3279-3284.

FREEZE, R.A., 1975, A stochastic-conceptual analysis of one-dimensional groundwater flow in nonuniform homogeneous media, Water Resources Research, v. 11 no. 5, pp. 725-741.

GALE, J.E., 1975, A Numerical Field and Laboratory Study of Flow in Rocks with Deformable Fractures, Ph.D. Thesis, University of California, Berkeley.

GANGI, A.F., 1978, Variation of whole and fractured porous rock permeability with confining pressure, International Journal of Rock Mechanics and Mining Sciences, v. 15, pp. 249-257.

GHABOUSSI, J. AND E.L. WILSON, 1971, Flow of Compressible Fluids in Porous Media, SESM Report No. 72-12, University of California, Berkeley.

GOODMAN, R.E., R.L. TAYLOR AND T. BREKKE, 1968, A model for the mechanics of jointed rock, Journal of Soil Mechanics and Foundation Division, ASCE, v. 94, no. SM3.

GREEN, A.E. AND P.M. NAGHDI, 1965, A dynamical theory of interacting continua, International Journal of Engineering Sciences, v. 3, pp. 231-241.

GRINGARTEN, A.C., H.J. RAMEY JR. AND R. RAGHAVAN, 1975, Applied pressure analysis for fractured wells, Journal Petroleum Technology, Transactions AIME, v. 259, pp. 887-892.

GURTIN, M., 1964, Variational principles for linear initial-value problems, Quarterly of Applied Mathematics, v. 22, no. 3, p. 252.

HELM, D.C., 1974, Evaluation of Stress-Dependent Aquitard Parameters by Simulating Observed Compaction from Known Stress History, Ph.D. Thesis, University of California, Berkeley.

HILBER, H.M., R.L. TAYLOR AND P.A. WITHERSPOON, 1979, Transient response of fractured rock systems to fluid injection: A finite element study, Proceedings of the Third International Conference on Numerical Methods in Geomechanics, Aachen.

HOCKING, G., 1979, Thermomechanical modeling for hardrock: Status and needs, in Proceedings Workshop on Thermomechanical Modeling for a Hardrock Waste Repository, Berkeley, California, Lawrence Livermore Laboratory Report UCAR-10043; ONWI-98, Livermore.

HUBBERT, M.K., 1956, Darcy's law and the field equations of the flow of underground fluids. Petroleum Transactions, AIME, v. 207, pp. 222-239.

HUDSON, J.A. AND S.D. PRIEST, 1979, Discontinuities and rock mass geometry, International Journal of Rock Mechanics and Mining Sciences, v. 16, pp. 339-363.

IWAI, K., 1976, Fundamental Studies of Fluid Flow Through a Single Fracture, Ph.D. Thesis, University of California, Berkeley.

KRANZ, R.L., A.D. FRANKEL, T. ENGELDER AND C. H. SCHOLZ, 1979, The permeability of whole and jointed Barre granite, International Journal of Rock Mechanics and Mining Sciences, v. 16, pp. 225-234.

LONG, J.C.S., J. REMER, C. WILSON AND P.A. WITHERSPOON, 1981, Porous media equivalent for a network of discontinuous fractures, submitted to Water Resources Research.

MAHTAB, M.A., D.D. BOLSTED AND J.R. ALLDREDGE, 1972, Analysis of Fracture Orientations for Input to Structure Models of Discontinuous Rock, U.S. Dept. of Interior, Bureau of Mines Report, Invest. N7669.

MARCUS, H. AND D. EVANSON, 1961, Directional Permeability in Anisotropic Porous Media, Water Resources Center Contribution No. 31, University of California, Berkeley.

MARCUS, H., 1962, Permeability of an anistropic porous medium, Journal of Geophysical Research, v. 67, p. 525.

NARASIMHAN, T.N., AND P. A. WITHERSPOON, 1977, Numerical model for saturated-unsaturated flow in deformable porous media, 1. Theory, Water Resources Research, v. 13, no. 3, pp. 657-664.

NOORISHAD, J., P.A. WITHERSPOON AND T.L. BREKKE, 1971, A Method For Coupled Stress and Flow Analysis of Fractured Rock Masses, Geotechnical Engineering Publication No. 71-6, University of California, Berkeley.

NOORISHAD, J, M. MEHRAN AND T.N. NARASIMHAN, 1981a, On the formulation of saturated-unsaturated fluid flow in deformable porous media, Advances in Water Resources (in press).

NOORISHAD, J. AND P.A. WITHERSPOON, 1981, Hydrothermoelasticity Part 1: Fundamentals and Analysis Approach, Lawrence Berkeley Laboratory Report LBL-12354, Berkeley.

NOORISHAD, J., P.A. WITHERSPOON AND M.S. AYATOLLAHI, 1981b, Coupled stress and fluid flow analysis of fractured rocks, submitted to International Journal of Rock Mechanics and Mining Sciences.

PARSONS, R.W., 1966, Permeability of idealized fractured rock, Society of Petroleum Engineers Journal, v. 6, pp. 126-136.

PINDER, G.F., 1979, State-of-the-Art Review of Geothermal Reservoir Modeling, Lawrence Berkeley Laboratory Report LBL-9093, Berkeley.

PRIEST, S.D. AND J. HUDSON, 1976, Discontinuity spacings in rock, International Journal of Rock Mechanics and Mining Sciences, v. 13, pp. 135-148.

RAGHAVAN, R., A. URAIET AND G. W. THOMAS, 1976, Vertical Fracture Height: Effect on Transient Flow Behavior, paper presented at 51st SPE-AIME meeting, New Orleans, October 3-6.

ROBERTSON, A, 1970, The interpretation of geological factors for use in slope stability, Proceedings Symposium on the Theoretical Background to the Planning of Open Pit Mines with Special Reference to Slope Stability, pp. 55-71.

ROCHA, M. AND F. FRANCISS, 1977, Determination of permeability in anisotropic rock masses from integral samples, In Structural and Geotechnical Mechanics, W. J. Hall (ed.), Prentice-Hall, Inc., New Jersey.

RODATZ, W. AND W. WITTKE, 1972, Wechselwirkung Zwischen Deformation und Durchströmung in Klüftigen, Anisotropen Gebirge, Proceedings of Symposium on Percolation Through Fissured Rock, Stuttgart, 1972, p. T2-1.

ROMM, E.S., 1966, Flow Characteristics of Fractured Rocks, Nedra, Moscow (in Russian).

SAFAI, N.M. AND G. F. PINDER, 1979, Vertical and horizontal land deformation in a desaturating porous medium, Advances in Water Resources, v. 2, pp. 19-25.

SANDHU, R.S. AND E.L. WILSON, 1969, Finite-element analysis of seepage in elastic media, Journal of Engineering Mechanics, Division ASCE, v. 95, no. EM3, p. 641-652.

SMITH, L., 1978, Stochastic Analysis of Steady State Groundwater Flow in a Bounded Domain, Ph.D. Thesis, University of British Columbia, Vancouver.

SMITH, L. AND R.A. FREEZE, 1979a, Stochastic analysis of steady state groundwater flow in a bounded domain, 1: One-dimensional simulations, Water Resources Research, v. 15, no. 3, pp. 521-528.

SMITH, L. AND R.A. FREEZE, 1979b, Stochastic analysis of steady groundwater flow in a bounded domain, 2: Two-dimensional simulations, Water Resources Research, v. 15, no. 6, pp. 1543-1559.

SNOW, D.T., 1965, A Parallel Plate Model of Fractured Permeable Media, Ph.D. Thesis, University of California, Berkeley.

SNOW, D.T., 1968, Fracture deformation and changes of permeability and storage upon changes of fluid pressure, Quartlery Colorado School of Mines, v. 63, no. 1, pp. 201.

SNOW, D.T., 1969, Anistropic permeability of fractured media, Water Resources Research, v. 5, no. 6, p. 1273.

SOREY, M.L, 1975, Numerical Modeling of Liquid Geothermal Systems, Ph.D. Thesis, University of California, Berkeley.

TAYLOR, R.L., 1974, Analysis of Flow of Compressible or Incompressible Fluids in Porous Elastic Solids, Consulting report to the Naval Civil Engineering Laboratory, Port Hueneme, California.

TERZAGHI, K., 1925, Erdbaumechanik auf Bodenphsikalischer Grundlage, Leipzig, F. Deuticke.

TOTH, J, 1967, Groundwater in sedimentary (clastic rocks), Proceedings of the National Symposium on Groundwater Hydrology, San Francisco, California, November 6-8.

TSANG, C.F., 1980, A review of the state-of-the-art of thermomechanical-hydrochemical modeling of a hardrock waste repository, Proceedings ONWI Workshop on Thermomechanical-Hydrochemical Modeling for a Hardrock Waste Repository, Berkeley, California, Lawrence Berkeley Laboratory Report LBL-11204, ONWI-164, Berkeley.

TSANG, Y.W. AND P.A. WITHERSPOON, 1981, Hydromechanical behavior of a deformable rock fracture subject to normal stress, submitted to Journal of Geophysical Research.

VENEZIANO, D., 1979, Probabilistic Model of Joints in Rock, Civil Engineering Department, Massachusetts Institute of Technology, Boston, 47 pp.

WALSH, J.B., 1965, The effect of cracks on the uniaxial elastic compression of rocks, Journal Geophysical Research, v. 70, pp. 399-411.

WANG, J.S Y., R. STERBENTZ AND C. F. TSANG, 1980, The State-of-the-Art of Numerical Modeling of Thermo-hydrologic Flow in Fractured Rock Masses, Lawrence Berkeley Laboratory Report LBL-10524, Berkeley.

WILSON, C.R. AND P.A. WITHERSPOON, 1970, An Investigation of Laminar Flow in Fractured Rocks, Geotechnical Report No.70-6, University of California, Berkeley.

ZIENKIEWICZ, O.C., 1971, The Finite Element Method in Engineering Science, McGraw-Hill, London.

APPENDIX

Initial and Boundary Conditions

The equations governing fluid flow (20), static equilibrium (22), and conservation of energy (23) in conjunction with the constitutive equations for the stress-strain relationships (19) and the equation of state for the fluid (21) have previously been discussed. These equations with the proper initial and boundary conditions define the problem to be solved. The initial and boundary conditions for the saturated porous elastic medium are:

$$\underline{U}(\underline{x}, t) = \hat{\underline{U}}(\underline{x}, t) \qquad \text{on } A_1 x[0, \infty)$$

$$\underline{\tau}(\underline{x}, t) \cdot \underline{n}(\underline{x}) = \hat{\underline{G}}(\underline{x}, t) \qquad \text{on } A_2 x[0, \infty)$$

$$P(\underline{x}, t) = \hat{P}(\underline{x}, t) \qquad \text{on } B_1 x[0, \infty)$$

$$\frac{\underline{k}_f}{\eta_\ell} \nabla(P + \rho_\ell g z) \cdot \underline{n}(\underline{x}) = \hat{Q}_\ell(\underline{x}, t) \qquad \text{on } B_2 x[0, \infty) \tag{A1}$$

$$T(\underline{x}, t) = \hat{T}(\underline{x}, t) \qquad \text{on } C_1 x[0, \infty)$$

$$K_M \nabla T \cdot \underline{n}(\underline{x}) = \hat{Q}_h(\underline{x}, t) \qquad \text{on } C_2 x[0, \infty)$$

$$\underline{U}(\underline{x}, 0) = 0 \qquad \text{on } V$$

$$\underline{\tau}(\underline{x}, 0) = 0 \qquad \text{on } V$$

$$P(\underline{x}, 0) = 0 \qquad \text{on } V \qquad \text{(A1)}$$

$$T(x, 0) = T_o \qquad \text{on } V$$

A, B, C represent parts of the boundary for stress-displacement, pressure-fluid flow, and temperature-heat flux considerations. V represents the volume under consideration. As mentioned earlier, the dependent variables $\underline{U}$, P and T represent incremental deviations from the strain-free state assumed by the above choice of initial conditions. Consideration of a different set of values for the initial conditions will necessitate replacement of $\underline{U}$, P, and T by $(U - U_o)$, $(P - P_o)$, and $(T - T_o)$ in all corresponding equations. Also τ has to change to $(\underline{\tau} - \underline{\tau}_o)$. However, to cause less manipulation, it is preferable that the displacement vector $\underline{U}$ be kept incremental in nature and left unchanged which will not affect the results of the analysis.

Variational Formulation

The variational method is used to formulate the hydroelastic [Ayatollahi, 1978] part of the hydrothermoelastic phenomena. Let $R = \underline{U}, P$ be an admissible state in J defined in $V \times [0, \infty)$ and let the functions $\underline{U}$ and P possess the appropriate continuity and differentiability conditions. J is the set of all admissible states and V is the region of space occupied by the fluid-porous solid mixture. A function $\Omega_t(R)$ over J for each time $t \in [0, \infty)$ is defined as:

$$\Omega_t(R) = \int_V (e_{ij} * C_{ijk\ell} e_{k\ell} - 2T * \beta\delta_{ij} e_{ij}$$

$$- 2\rho_s f_i * U_i + 2P * \frac{\alpha\rho_\ell}{\rho_o}\delta_{ij} e_{ij}$$

$$- 1 * \nabla P * \frac{k_f}{\eta_\ell}\nabla P - P * \frac{1}{M} P - P * \frac{1}{M_T} T$$

$$+ 2 * \rho_\ell g \nabla z * \nabla P) dv - 2\int_{A_2} \hat{G}_i * U_i ds$$

$$- 2\int_{B_2} 1 * \hat{Q}_\ell * P ds \qquad \text{(A2)}$$

It can be shown that

$$\delta_R \Omega(R) = \frac{d}{d\nu}\Omega(R + \nu\bar{R})\Big|_{\nu=0} = 0 \qquad \text{(A3)}$$

for every $R \in J$ if, and only if, R is a solution state of the mixed boundary-value problem. The presence of temperature terms in the variational principle is justified physically, besides the mathematical soundness of the formulation, by the fact that thermal effects act in the form of initial strains (Zienkiewicz, 1971).

Galerkin formulation

The Galerkin method is used to obtain a numerical formulation for the energy equation. Choosing approximating functions of the form $T = \underline{\Phi}\underline{T}$, where Φ_i represents the basis functions and T_i signifies the discrete temperature values to be determined, the Galerkin procedure requires the following:

$$\int_V \Big\{ (\rho C)_M \Phi_i \frac{\partial T}{\partial t} + \beta T_o \Phi_i \frac{\partial}{\partial t}(\delta_{ij} e_{ij})$$

$$+ \rho_\ell C_{v\ell} \Phi_i \underline{q} \cdot \nabla T + \nabla\Phi_i \cdot K_M \nabla T \Big\} dv$$

$$- \int_{C_2} \Phi_i \hat{Q}_h ds = 0 \qquad \text{(A4)}$$

where the volume integral in equation (A4) represents a global restatement of (23), and the surface integral indicates the global satisfaction of the heat flux boundary condition.

Finite-Element Discretization

The field variables for the displacement vector, the pressure, and the temperature can be discretized as follows:

$$\underline{U} = \underline{\Phi}_U^{T_r}\underline{U}$$

$$P = \underline{\Phi}^{T_r}\underline{P} \qquad \text{(A5)}$$

$$T = \underline{\Phi}^{T_r}\underline{T}$$

where the Φ_i are piecewise continuous polynomial functions which are used in conjunction with the mixed isoparametric quadrilateral elements. Proper substitution of equation (A5) and related derivatives of $\underline{\Phi}_u$ and $\underline{\Phi}$ represented by $\underline{\Phi}_e$ and $\underline{\Phi}_\theta$ in the Galerkin integral and the functional, after proper differentiation, yields the following matrix finite element formulation:

$$\underline{K}\,\underline{U} + \underline{C}_{UP}\underline{P} + \underline{C}_{UT}\underline{T} = \underline{F} \qquad \text{(A6)}$$

$$\underline{C}_{PU}\underline{U} + (\underline{E}_f + 1^*\underline{H}_f)\underline{P} + \underline{C}_{PT}\underline{T} = -1^*\underline{Q}_\ell \qquad \text{(A7)}$$

$$\underline{C}_{TU}\underline{U} + [\underline{E}_h + 1^*(\underline{H}_{hf} + \underline{H}_h)]\underline{T} = -1^*\underline{Q}_h \qquad \text{(A8)}$$

where 1^* represents time integration. The matrix coefficients in the above formulation are defined by the following:

$$\underline{K} = \sum_{n=1}^{N} \int_{v^n} \underline{\Phi}_e^{n} \underline{C}^{n} \underline{\Phi}_e^{n\,T_r} dv^n$$

$$\underline{C}_{PU} = \underline{C}_{UP}^{T_r} = \sum_{n=1}^{N} \int_{v^n} \underline{\Phi}^n \frac{\alpha^n \rho_\ell^n}{\rho_o} \hat{1}\, \underline{\Phi}_e^{n\,T_r} dv^n$$

$$\underline{C}_{UT} = \sum_{n=1}^{N} \int_{v^n} \underline{\Phi}^n \beta \hat{\underline{1}} \, \underline{\Phi}_e^{n\,T_r} dv^n$$

$$\underline{C}_{TU} = \frac{1}{T_o} \underline{C}_{UT}^{T_r}$$

$$\underline{E}_f = \sum_{n=1}^{N} \int_{v^n} \underline{\Phi}^n \frac{1}{M^n} \underline{\Phi}^{n\,T_r} dv^n$$

$$\underline{H}_f = \sum_{n=1}^{N} \int_{v^n} \underline{\Phi}_\theta \frac{\underline{k}_f^n}{\eta_\ell} \underline{\Phi}_\theta^{T_r} dv^n$$

$$\underline{C}_{PT} = \sum_{n=1}^{N} \int_{v^n} \underline{\Phi}^n \frac{1}{M_T^n} \underline{\Phi}^{n\,T_r} dv^n$$

$$\underline{E}_h = \sum_{n=1}^{N} \int_{v^n} \underline{\Phi}^n (\rho C)_M^n \underline{\Phi}^{n\,T_r} dv^n$$

$$\underline{H}_{hf} = \sum_{n=1}^{N} \int_{v^n} \underline{\Phi}^n (\varepsilon \rho_\ell \, C_{v\ell})^n \underline{q} \, \underline{\Phi}_\theta^{n\,T_r} dv^n$$

$$\underline{H}_h = \sum_{n=1}^{N} \int_{v^n} \underline{\Phi}_\theta^n \underline{K}_M^n \underline{\Phi}_\theta^{T_r} dv^n$$

$$\underline{Q}_\ell = \sum_{n=1}^{n_1} \int_{B_2^n} \underline{\Phi}^n \underline{\Phi}^{n\,T_r} \hat{Q}_f^n ds^n$$

$$+ \sum_{n=1}^{N} \int_{v^n} \underline{\Phi}_\theta \frac{\underline{k}_f^n}{\eta_\ell} \rho_\ell g \hat{\underline{1}}_z dv^n$$

$$\underline{Q}_h = \sum_{n=1}^{n_2} \int_{C_2^n} \underline{\Phi}^n \underline{\Phi}^{n\,T_r} \hat{Q}_h ds^n$$

$$\underline{F} = \sum_{n=1}^{n_3} \int_{A_2^n} \underline{\Phi}_u^n \underline{\Phi}_u^{n\,T_r} \hat{\underline{G}} \, ds^n$$

$$+ \sum_{n=1}^{N} \int_{v^n} \underline{\Phi}_u \rho_s^n g \, \hat{\underline{1}}_z dv^n$$

where $\hat{\underline{1}} = \begin{Bmatrix} 1 \\ 1 \\ 1 \\ 0 \\ 0 \\ 0 \end{Bmatrix}$ and $\hat{\underline{1}}_z = \begin{Bmatrix} 0 \\ 0 \\ 1 \end{Bmatrix}$

The superscript T_r stands for matrix transposition operation.